THE JOURNAL OF PHYSICAL CHEMISTRY B

Article

pubs.acs.org/JPCB

Molecular Dynamics Simulation of Phosphoric Acid Doped Monomer of Polybenzimidazole: A Potential Component Polymer Electrolyte Membrane of Fuel Cell

Swagata Pahari,[†] Chandan Kumar Choudhury,[†] Prithvi Raj Pandey,[†] Minal More,[‡] Arun Venkatnathan,[‡] and Sudip Roy*,[†]

[†]Physical Chemistry Division, National Chemical Laboratory, Pune 411008, India

[‡]Department of Chemistry, Indian Institute of Science Education and Research, Pune 411021, India

Supporting Information

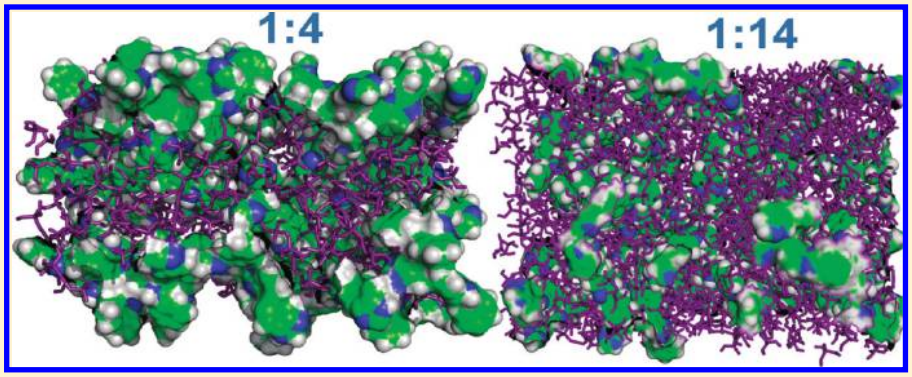

ABSTRACT: Phosphoric acid doped polybenzimidazole is promising electrolyte membranes for high temperature (100 °C and above) fuel cells. Proton conduction is governed by the amount of phosphoric acid content in the polymer membrane. In this present work, we perform molecular dynamics simulations on phosphoric acid doped 2-phenyl-1*H*,1′*H*-5,5′-bibenzo[*d*]imidazole (monomer unit of polybenzimidazole) to characterize the structural and dynamical properties at varying phosphoric acid content and temperature. From the structural analysis, we have predicted the arrangement of the phosphoric acids, formation of H-bonds in the system, and the contribution of different atoms toward H-bonding. We have also examined the stacking of 2-phenyl-1*H*,1′*H*-5,5′-bibenzo[*d*]imidazole molecules and how their arrangement changes with the increasing amount of PA in the system with the help of cluster analysis. From the molecular dynamics simulation conducted at different temperatures and phosphoric acid doping level, we have predicted the diffusion of phosphoric acid and monomer. As a dynamic quantity, we have also calculated ring flipping of the imidazole ring of the monomer.

INTRODUCTION

Polymer electrolyte membrane fuel cell (PEMFC) can generate power with high efficiency and minimal pollution[1] and have various applications in aerospace, military,[2] transportation, and stationary applications.[3] The polymer electrolyte membrane (PEM) is an important constituent of PEMFC. It plays a crucial role in determining the efficiency of a fuel cell by selectively transporting protons from anode to cathode. The polymer membrane has three functions: (a) as an electrolytic medium for proton conduction, (b) as a barrier for separating reactant gases, e.g., hydrogen on anode and oxygen on cathode, and (c) as a support for electrode catalysts. To satisfy these purposes, the membrane should possess high ionic conductivity, low gas permeability, and good mechanical strength.[4] The most widely experimentally[5−8] and theoretically[9−11] characterized membrane is the Nafion membrane. This particular membrane needs to be solvated with water for better proton conduction, which is directly related to the degree of hydration of the membrane.[12] Thus, the operating temperature of the fuel cell, which uses the Nafion membrane, is limited by the boiling temperature of water. Above this temperature, proton conductivity of the membrane decreases due to the evaporation of water,[13] and hence, efficiency of the cell decreases. Taking into consideration some economical challenges such as production and storage of fuel, water-thermal management, fast electrode kinetics, and increased tolerance to impurities in the PEMFC system, increasing attention is drawn for choosing membranes, which can function at elevated temperatures.[14,15] Various PEM, which can work at higher temperature, have been proposed[3,16−18] and reviewed by Li et al.[19] The phosphoric acid (PA) doped[20−22] polybenzimidazole (PBI) was found to be one of the promising candidates. The use of PBI as a membrane

Received: February 3, 2012
Revised: May 23, 2012
Published: May 31, 2012

   dx.doi.org/10.1021/jp301117m | *J. Phys. Chem. B* 2012, 116, 7357−7366

for fuel cell was first introduced by Wainright et al.,[23] who showed that acid doped PBI can be used as replacement of the Nafion membrane and can conduct proton at high temperature (110 °C without external humidification). Beside this, PBI has been observed to possess many favorable properties such as high glass transition temperature (T_g = 698−708 K),[4] good chemical resistance,[24] excellent textile fiber properties,[25] and good proton conductivity after being doped with PA.[26] Therefore, it can act as a potential candidate to be used in a PEMFC. The high temperature stability of the doped acids and the affinity between PA and PBI molecules have been a matter of concern, as enough acid doping level is necessary for introducing PBI membranes in PEMFCs.[27] Numerous experimental studies have been performed on the PA doped PBI membrane concerning its proton conductivity.[12,28−30] For the PBI/PA system, proton conductivity strongly increases in a nonlinear fashion with an increasing amount of PA, while the mechanical strength decreases significantly.[21,30,31] It was observed that increasing the doping level of PA from 3.28 to 4.62 mol per polymer repeat unit, the proton conductivity increases from 0.020 to 0.060 S cm^{-1}. However, the tensile strength decreases from 121 to 33 MPa.[30] Hence, a doping level of 5−6 mol of PA per mol of polymer repeat unit is reported to obtain good conductivity maintaining a reasonable mechanical strength of the membrane.[21] Recently, Xiao et al.[29] developed a sol−gel process in which doping was achieved through the hydrolysis of polyphosphoric acid to PA. The doped membrane contained 20−40 mol of PA per mol of PBI repeat unit, and it acquired good mechanical properties at higher temperatures. For a given doping level, the conductivity increases with temperature. For example, it was reported that the PBI/PA membrane exhibits proton conductivity of 5 × 10^{-3} S cm^{-1} at 298 K, which increases to 4 × 10^{-2} S cm^{-1} at 190 °C.[28]

Pure PA has been found to be one of the high proton conduction media at higher temperature (150−200 °C)[32] since the boiling point of PA is 213 °C. Proton transport in PA doped PBI membranes is thought to involve two mechanisms: (a) proton shuttling among solvent molecules (PA) via Grotthuss mechanism and (b) vehicular transport mechanism where protons diffuse in solution in the form of prorogated PA.[33] The advantage of PA is that it can conduct proton in anhydrous form[34,35] due to its proton-solvating ability and self-ionization behavior.[36] Pure bulk PA self-dissociates and generates equilibrium between orthophosphoric acid and pyrophosphoric acid. Munson[37] had shown that, at high temperature, the molten PA system contains $H_4PO_4^+$, $H_2PO_4^-$, H_3O^+, and $H_2P_2O_7^{2-}$. However, Munson in the same report had experimentally proved that the time scale to achieve such equilibrium is more than 3 weeks, even at high temperature. Recently, Kreuer et al. reported[38] by performing an ab initio molecular dynamics simulation that pure PA bulk shows Grotthuss-like proton conductivity, which occurs due to interplay between the hydrogen bonded chains of PA and the frustrated hydrogen bond network. They have also shown that, in PA, the hydrogen bonds are short and strong and that self-dissociated ions get fused when they encounter each other. Because of the strong hydrogen bonds and oppositely charged species, the PA molecules will stay together.

PBI is amorphous in nature and shows a high degradation temperature, which makes it an excellent PEM at elevated temperature. The higher acid uptake ability[27,28] of PBI also stands in favor of its usage as a proton exchange membrane material.

In the present study, we report the structural and dynamical properties of 2-phenyl-1*H*,1′*H*-5,5′-bibenzo[*d*]imidazole (BI) (Figure 1a), the monomeric unit of PBI mixed with PA using

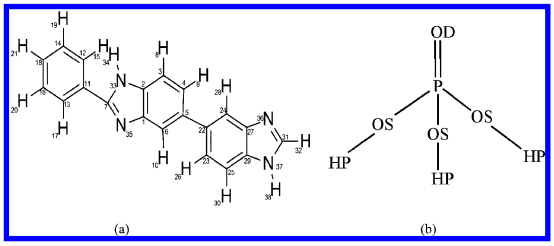

Figure 1. (a) Structure of monomer unit of PBI (BI). (b) Structure of PA.

classical all atomistic molecular dynamics (MD) simulation. Three different systems, which consist of different amounts of PA to cover the whole experimental spectrum of doping level, have been studied here. In addition, pure PA and pure BI simulations have also been performed to observe the effect of doping on both BI and PA. The BI to PA ratio was varied in the mixed systems as 1:4, 1:8, and 1:14. It is well accepted that the conductivity of PA doped PBI membrane increases with an increasing amount of PA in the system at higher temperatures.[30] To the best of our knowledge, no optimized force field exists for the monomer BI or the polymer PBI. Therefore, we have calculated few parameters for the force field, e.g., charges and dihedral angles for BI, and adopted other parameters from literatures. The force field used in the present work can be further tuned and used for the polymeric PBI system. The main motivation for the present study is to understand the molecular level structural arrangements of BI and PA molecules, which is directly correlated to the conduction of protons. Such understanding at the molecular level is still missing and highly desirable in the fuel cell community. Though the polymeric form of BI, i.e., PBI, has not been considered in the present study, this work on the BI−PA mixtures will be one of the first attempts to model such system. The monomer of PBI also serves the purpose of understanding the underlying mechanism of diffusion of PA in the presence of BI and vice versa. It is difficult to perform classical MD simulations with all possible types of phosphate ions as mentioned above because of limitations in force fields. The optimization of force field for individual ions are challenging because of nonavailability of enough experimental observables. Therefore, this report gives ample results for a model system, which we believe can give a well representative picture of PA and BI mixed system. There is enough scope for further improvement of our model.

The rest of the article is organized as follows: the computational details are presented in the following section. The structural and dynamical properties of PA doped BI are described in the results and discussion section. A summary of salient results concludes this article.

■ COMPUTATIONAL DETAILS

We have performed MD simulation using all atom force-field on systems: pure BI, pure PA, and BI mixed with varying amounts of PA. The chemical structures of BI and PA are shown in Figure 1a,b, respectively. All simulations were performed with the GROMACS 4.0.7 package.[39,40] A

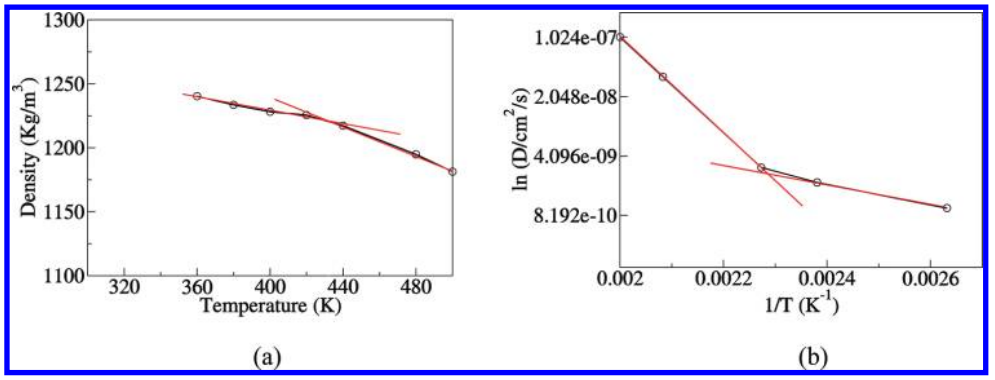

Figure 2. (a) Density as a function of temperature. (b) Natural log of diffusion as a function of inverse temperature for BI.

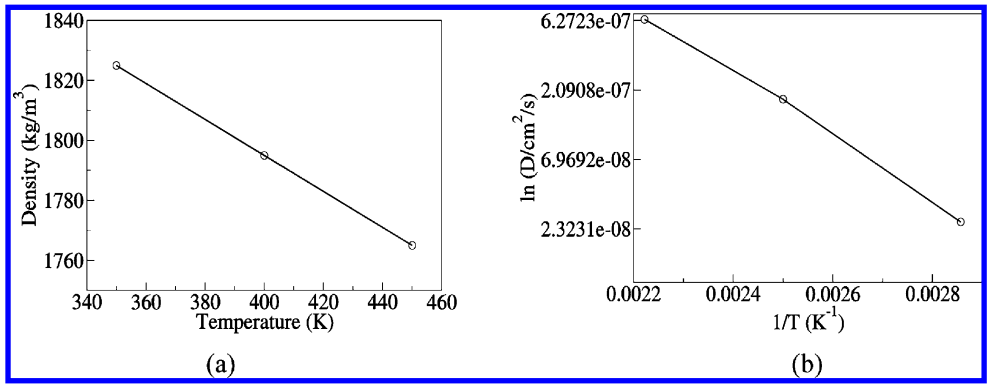

Figure 3. (a) Density as a function of temperature. (b) Natural log of diffusion as a function of inverse temperature for PA.

simulation cell containing 125 molecules of BI was constructed for pure BI. For pure PA, 1000 molecules were simulated. In mixed systems, a fixed amount of monomer, i.e., 64 molecules of BI, were mixed with PA in three different ratios: 1:4, 1:8, and 1:14 according to the number of molecules, i.e., per monomer molecule.

Force Field. The total potential energy used in the simulation is the sum over all intramolecular and intermolecular interactions. The intramolecular interaction energy consists of harmonic bond, angle potential, and proper and improper dihedral potential. The nonbonded interactions energy consists of Lennard-Jones potential and electrostatic interaction. All these potential energy forms were used as implemented in GROMACS.

The bond and angle potential parameters for BI were taken from the OPLS-AA force field.[41,42] The calculation of dihedral potentials for BI were done as follows: we optimized the BI molecule using the Hartree−Fock method with 6-311g basis set by using the Gaussian09 program.[43] A dihedral scan was performed for 20 steps with an increment of 18° in each step. At each step, the geometry of the molecule was optimized, and the energy value was calculated as a function of dihedral angle and fitted by the dihedral potential function of the form

$$V = \sum_{p} \frac{k_{\tau_p}}{2}[1 - \cos p(\varphi - \varphi_0)]$$

where k_{τ_p} is the dihedral force constant, φ is the corresponding dihedral angle, φ_0 is the equilibrium dihedral angle, and p is the periodicity. The calculated parameters (force constant, dihedral angle, and periodicity) were fed in the force-field topology. In Figures SI1a,b, Supporting Information, the dihedral energies from ab initio quantum chemical calculation and fitting of the classical dihedral potential energy function have been shown for $C_4-C_5-C_{22}-C_{23}$ and $C_{12}-C_{11}-C_7-N_{35}$ (numbering of the atoms are according to Figure 1a) dihedrals, respectively. The values of Lennard-Jones parameters (σ and ε) were taken from the OPLS-AA force field. The partial charges of the individual atoms are calculated by quantum chemical calculation using the Gaussian09 code.[43] For this purpose, after geometry optimization, we used the CHELPG[44] method to calculate the partial charges for all the individual atoms of BI. All bonded force field parameters including the parameter adopted from OPLS-AA for BI are listed in Table SI1 of the Supporting Information. The calculated charges for all the atoms of BI are given in Table SI2 of the Supporting Information.

For all simulations, the NPT ensemble and periodic boundary conditions were used. Temperature was kept constant using a Berendsen thermostat.[45] A Berendsen barostat was used to keep the pressure constant at 1 bar. Reaction field electrostatics[46,47] was used with a cutoff length of 1 nm. For pure PA, 20 ns production runs were performed at 400, 450, and 500 K. We prepared the system of pure BI at 500 K and cooled down in steps of 20 K up to 400 K. At all these intermediate and final temperatures, a 50 ns production run was performed. In the case of mixed systems, simulated annealing for better sampling of the phase space on the energy optimized structure was performed as follows: the initial structures of the mixed systems were taken at 400 K. The systems were gradually heated from 400 to 700 K, by 100 K in each step, and a NPT simulation for 100 ps was performed at each step. Similarly, the system was cooled in three steps from 700 to 400 K. This cycle of heating and cooling was repeated six times. From this cycle, we picked up three mixed systems at three different temperatures (400 K, 450 K, and 500 K), and

dx.doi.org/10.1021/jp301117m | J. Phys. Chem. B 2012, 116, 7357−7366

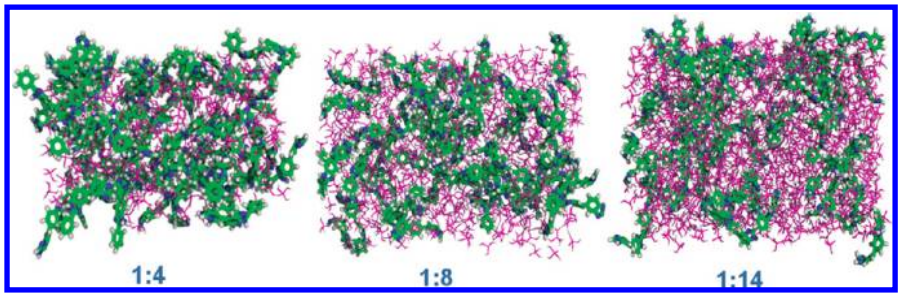

Figure 4. Snapshots of BI−PA mixed systems (1:4, 1:8, and 1:14).

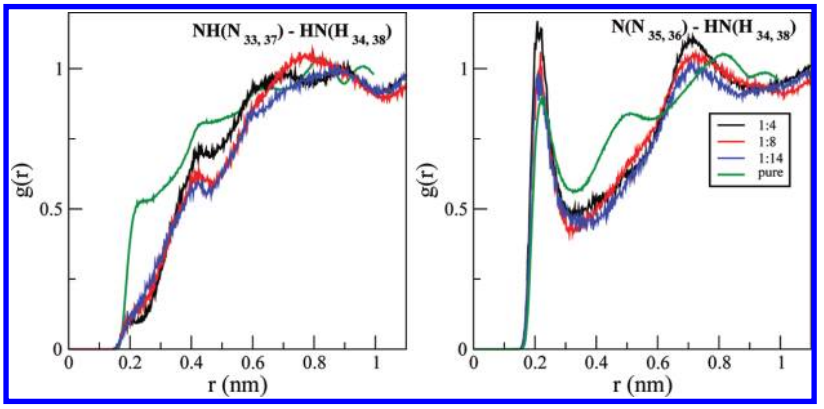

Figure 5. RDF between different atoms of BI molecules.

then, NPT simulations for 50 ns were performed at these temperatures. Although we performed the simulation at three different temperatures, we have given the structural insight of all the systems only at 500 K, as the effect of temperature on the structural arrangement observed is not significant.

Force Field Validation. The validation of force field was performed by calculation of density and diffusion coefficient of the pure systems. The calculated density of pure PA at 298 K and 1 atm pressure is found to be 1.855 g/cm^3 and is slightly lower than the experimental value of 1.868 g/cm^3.[11] For pure BI, the calculated density is 1.245 g/cm^3 at 300 K, whereas the reported experimental density is 1.33 g/cm^3 for polymeric BI (PBI), at 308 K and 1 atm.[48] The calculated densities at different temperatures for BI and PA are plotted in Figures 2a and 3a, respectively. In the case of pure BI, below 440 K, the rate of increase in density with a decrease in temperature is less (Figure 2a). Hence, this particular temperature, i.e., 440 K is near to the glass transition temperature for BI. However, for PBI, the glass transition temperature is reported to be 693 K.[4] From Figures 2a and 3a, we have also calculated the thermal expansion coefficient value for BI and pure PA, respectively, using the following relationship:

$$\alpha = -\frac{1}{\rho}\frac{\partial \rho}{\partial T}$$

where α is the thermal expansion coefficient, ρ is the initial density, and $(\partial\rho/\partial T)$ is the density change with respect to temperature. The slopes of the Figures 2a and 3a plots give us $(\partial\rho/\partial T)$ for BI and PA, respectively. For BI, slope was taken above the glass transition temperature (440 K). Dividing the slope by the initial density ρ, we obtained the thermal expansion coefficient. The thermal expansion coefficient at 500 K temperature for BI was calculated to be 50×10^{-5} K^{-1} and for PA is 34×10^{-5} K^{-1}.

The calculated diffusion coefficients (D) for pure BI and pure PA at different temperatures are plotted in Figures 2b and 3b. From the Arrhenius plot (ln D as function of $1/T$), we observed in the case of pure BI, deviation from linearity appears below 440 K (see Figure 2b). Therefore, the density and diffusion values show that around 440 K is the glass transition temperature for BI. However, for pure PA, density gradually increases with a decrease in temperature (Figure 3a) and unlike pure BI, the plot of ln D vs $1/T$ for pure PA (Figure 3b) is linear, which shows that diffusion of PA increases with an increase in temperature. Density and diffusion values of PA have been checked for larger system containing 2000 PA molecules. The values are almost same. The density and diffusion plot as a function of temperature for this larger system are given in the Supporting Information in Figure SI4. From the Arrhenius plot, we calculated the activation energy for pure BI and pure PA using the following equation:

$$\ln D = \ln A - \frac{E_a}{RT}$$

The activation energy of pure BI was calculated to be 58 kJ/mol and for pure PA to be 44 kJ/mol. Since no experimental data for BI is available in the literature, validation of the calculated properties is done with the polymeric form of BI (PBI). The calculated density of BI is 6.4% lower than the density of PBI, which is within the limit of deviation of density for a monomer to polymer transition.

RESULTS AND DISCUSSION

The primary motivation of the present work is to understand the structural and dynamical properties of the BI in the presence of PA. Different PA content can change the structural arrangement of the BI matrix, which is directly correlated to the hydrogen bond network formation in the system. Diffusion

dx.doi.org/10.1021/jp301117m | J. Phys. Chem. B 2012, 116, 7357−7366

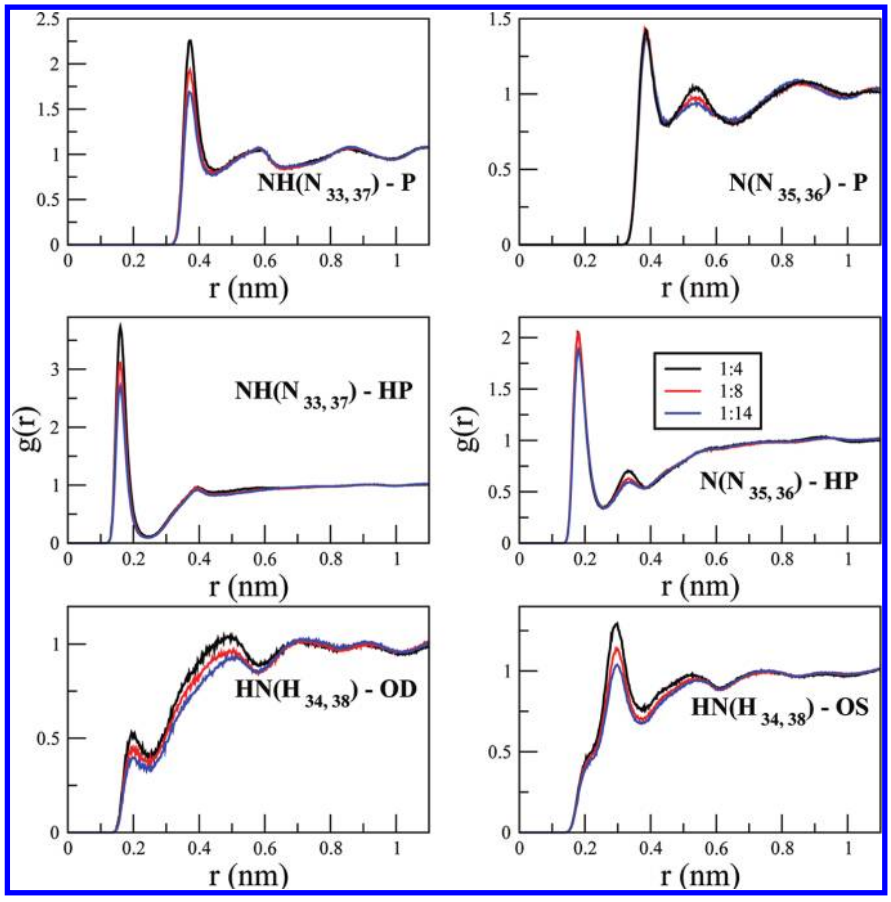

Figure 6. RDF between various atoms of BI and PA molecules.

mechanism of PA in the matrix of BI at different temperatures and different mixing ratios are related to the proton conduction by the hopping mechanism.

Structural Properties. The snapshots for all mixed systems are shown in Figure 4. A visual inspection of the snapshots shows that there is no clear phase separation of BI and PA. This confirms that most of the BI molecules are in contact with PA. We have also performed a NPT simulation for a 1:4 system containing a larger amount of BI and PA (512 BI and 2048 PA) to check the size effect on the phase morphology. In this case, also, we do not observe any distinct phase separation (Figure SI3, Supporting Information). This indicates that the phase morphology of the systems studied is independent of the system size. To investigate the structural arrangements of the BI in the mixed systems compared to the pure BI system, the radial distribution functions (RDF) have been calculated between various atoms of BI. The intermolecular RDFs were plotted between the amine nitrogen (NH, i.e., N_{33} and N_{37} according to Figure 1a) and the hydrogen attached to nitrogen (HN, i.e., H_{34} and H_{38} in Figure 1a), and between the imine nitrogen (N, i.e., N_{35} and N_{36}) and HN for pure and all mixed systems. An examination of the NH−HN RDFs shows no clear peaks for any of the systems (Figure 5). However, it indicates some distinctions in the arrangement of the BI molecules on going from pure BI to the mixed systems containing a different percentage of PA.

The first peaks in the N−HN RDF (Figure 5) show the minima at 0.3 nm, which is well inside the hydrogen bonding distance criteria. This is the indication of the presence of intermolecular hydrogen bonding interactions between BI molecules. The peak height is higher in the mixed systems compared to the pure BI system. This signifies higher ordering of BI molecules in the mixed systems compared to the pure BI system. The RDF peak height is the lowest for pure BI and the highest for the 1:4 system. Further, the peak height decreases as we go to a higher PA ratio. The 1:4 system shows better ordering for BI molecules than the others. The presence of PA induces the BI molecules to come closer to PA and with an increment in the percentage of PA in the mixed systems, a greater number of PA gets structured around BI. Therefore, the number of BI molecules arranging around each other decreases. The H-bonding among N and HN is an important aspect for such an arrangement.

The structural arrangements of the PA molecules around BI are investigated by checking the RDFs between N, HN, and NH atoms of BI and various atoms of PA for all the mixed systems and depicted in Figure 6. Since PA acts as a solvent in the PEM, an investigation of the structural arrangements of PA around BI will provide insights on favorable interaction sites and hence the formation of hydrogen bond networks between the two components. The RDFs of NH with phosphorus of PA (P) and between N and P signify clustering of PA molecules around imidazole moiety of the BI. There is a drop in the peak height of the NH−P RDFs with an increase in the amount of PA, which shows that ordering of PA molecules around the NH sites of BI is higher at a lower doping level of PA. However, there is not much shift in the peak heights in N−P RDFs with varying the amount of PA. Thus, the ordering of PA molecules around the N site of BI is not affected much with an increase in the amount of PA. The RDFs between NH and HP (hydrogen

dx.doi.org/10.1021/jp301117m | J. Phys. Chem. B 2012, 116, 7357−7366

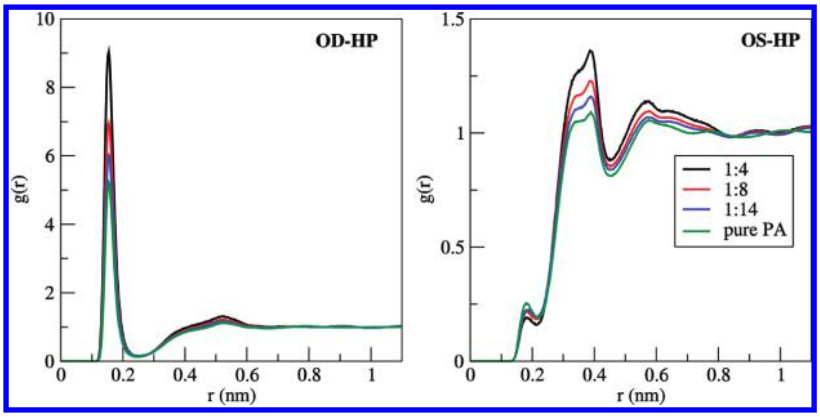

Figure 7. RDF between different atoms of PA molecules.

on PA) and also between N and HP are shown in Figure 6. These RDFs show the extent of H-bonding interactions between BI and PA. Fairly sharp RDF peaks can be observed with the first minima at the H-bonding distance for all ratios of the mixed systems. This suggests that the PA molecules have an ordered arrangement in order to undergo H-bonding with BI. The NH−HP RDFs peaks, and hence the H-bonding interaction decreases with the increase in the amount of PA, but the extent of H-bonding between N and HP is not affected much with a change in the BI to PA ratio. The possibility of the existence of H-bonding is further investigated by calculating RDFs between HN and single bonded oxygen of PA (OS) and double bonded oxygen of PA (OD). RDF peaks between HN and OD are broad and decrease with an increase in the BI to PA ratio. On the contrary, almost no peak at the H-bonding distance is observed for the HN and OS RDF plots. This is rather surprising because both the nitrogen atoms of BI (i.e., NH and N) actively take part in H-bonding interaction, but the extent is much less for double bonded oxygen (OD) and almost nothing for single bonded oxygen (OS) of PA. This is possibly because the highly ordered arrangement of HP atoms around NH hinders the HN and OS to set the proper alignment to undergo H-bonding.

Intermolecular RDFs are also calculated between OD and OS with HP of PA in the mixed systems and compared with the pure PA system (Figure 7). The peak heights of the RDF plots between OD and HP decrease steadily with an increase in the amount of PA in the mixed systems. Peak height is lowest for the pure PA system. It shows that PA forms an H-bonding network (minima of the first peaks are at 0.24 nm) in the mixed system and that this network is better ordered compared to the pure PA system. Further, there is not much change in the first peak heights of the RDF plots between OS and HP, showing that there is not much change in the H-bonding among these atoms with a change in percentage of PA.

Clustering of BI Molecules in PA Doped BI Mixtures. Analysis of the RDF plots showed that a greater number of BI molecules becomes ordered around each other with an increase in the amount of PA for the mixed systems. To verify this, the clustering of BI molecules has been investigated. To identify the clustering among the BI molecules, the distance between the center of masses (COM) among all the BI molecules were first computed. All the BI molecules for which the distance between the COMs came within 0.95 nm were considered to be a single cluster. This particular distance, 0.95 nm, is the distance of the second solvation shell of a BI molecule (taken from the RDF between BI molecules in pure system, not shown in this article), i.e., until this distance, there is probability of a BI molecule to be near the other BI molecules and form a cluster. The cluster sizes, with respect to number of BI molecules, were calculated in each frame of the trajectory separately for all the mixed systems at only 500 K. Finally, the number of occurrences of the cluster sizes, sampled over last 10 ns trajectory, is plotted in Figure 8. A higher number of

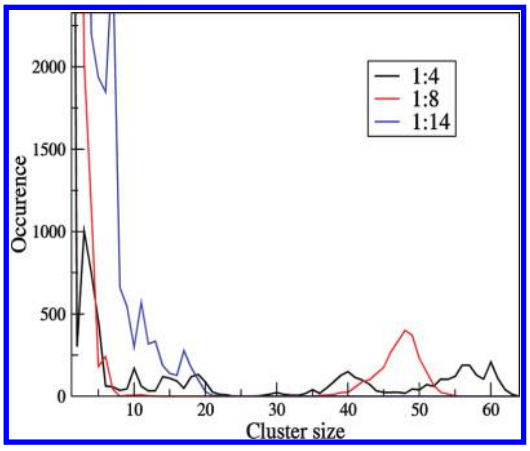

Figure 8. Cluster analysis of BI molecules in mixed systems.

occurrence at a particular cluster size value indicates higher probability of formation of cluster of that size in the 10 ns time window. The cluster size of one has the highest occurrence for all the mixed systems, which is obvious because each frame may have few isolated molecules. Figure 8 shows that, from smaller to higher PA ratio, the number of occurrence of smaller sized clusters increases. Larger sized clusters (cluster size more than 20) are almost absent in case of the 1:14 system, but for 1:8 and 1:4 systems, it occurs several times. The probable reason may be in the case of the system with a higher amount of PA; BI is surrounded by a larger number of PA molecules, and because of the favorable H-bonding interaction between PA and BI, BI molecules cannot phase separate completely to become clustered. A snapshot of such situation is provided in Figure 9, which shows that PA molecules are interpenetrated in the clusters of BI molecules. However, in the cases of 1:4 and 1:8 BI−PA systems, there are BI clusters, which are large in size but with much less occurrence. As BI clusters are small in size, a continuous proton transport pathway is generated through the intermolecular H-bonding network between PA molecules and also between PA and BI molecules. Since proton transfer

dx.doi.org/10.1021/jp301117m | J. Phys. Chem. B 2012, 116, 7357−7366

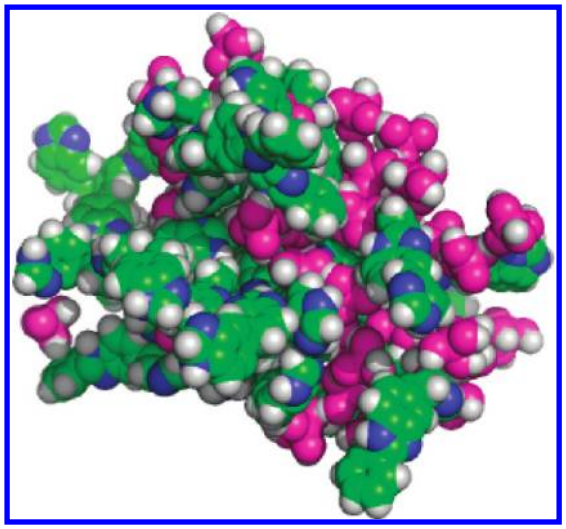

Figure 9. Snapshot of PA entering in between BI clusters.

hopping between two molecules follows the following order, $H_3PO_4\cdots H_2PO_4^-$ > $N-H^+\cdots H_2PO_4^-$ > $N-H^+\cdots N-H$, as reported by Ma et al.,[49] the contribution of PA dynamics toward long-range proton transport is more than BI;[33] hence, we can expect that, with decreasing the size of the BI cluster as well as increasing the PA−PA association, the proton transfer rate should increase.

Arrangement of Clustered BI Molecules: Stacking. The clustering of BI molecules is observed to decrease with an increase in the amount of PA in the mixed systems. The hopping mechanism of the proton in a PEMFC is strongly dependent upon the arrangement of PBI molecules and also upon the arrangement of PA molecules around it. So the understanding of the arrangement of BI molecules at the structural level would better equip us to deal with the structural arrangements and proton conduction mechanism in the polymeric system. Hence, the issues of how the BI molecules are arranged in the clustered structure and how the arrangement changes with the change in the amount of PA in the mixed systems are important to address. To calculate the arrangement, a vector between H_{21} and H_{32} (see Figure 1a) of all the BI molecules of the system was defined. Then, the angle between these vectors for the BI molecules falling within a distance of 0.95 nm was computed in each frame of the trajectory. The distance criteria were given with respect to the COM of the BI molecules as in the case of cluster calculations. Finally, a distribution was plotted from all these angles normalized over a number of BI molecules falling within 0.95 nm and a number of frames (Figure 10). This angle distribution was calculated over last 10 ns of the trajectory. A broad distribution can be observed for all the systems ranging from 0° to 180° with small humps. Two broad peaks can be observed for the pure, 1:4, and 1:8 systems. Also the peaks are more prominent for the 1:4 and 1:8 systems as compared to the pure BI system. This indicates the presence of two different conformations in two mixed systems. Also, the probability of these conformations becomes more significant in the 1:4 and 1:8 systems compared to the pure system. Thus, it can be inferred that the presence of PA caused biasness toward these conformations for BI molecules. However, for the 1:14 system, only one distinct hump can be observed near 150°. Thus, at the highest doping level of PA, at which conductivity has been observed to be maximum, the BI molecules prefer to remain in

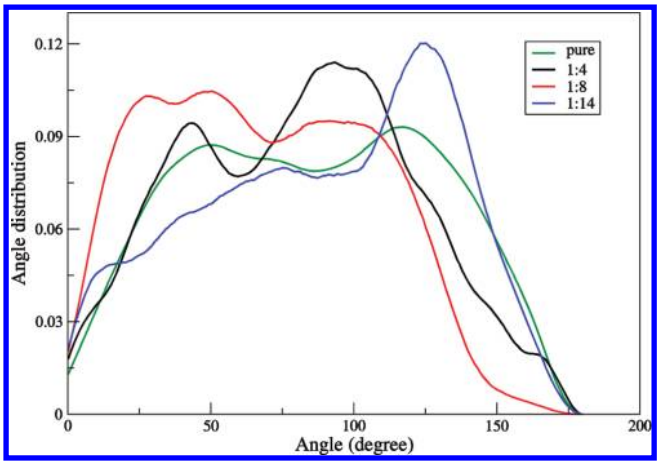

Figure 10. Angle distribution for BI molecule in pure BI and all the mixed systems.

a nearly parallel conformation with respect to each other. To better visualize the conformational biasness, snapshots extracted from real time trajectory containing two BI molecules in nearly parallel and nearly perpendicular arrangements are depicted in Figure 11. This distinction in the BI molecule from

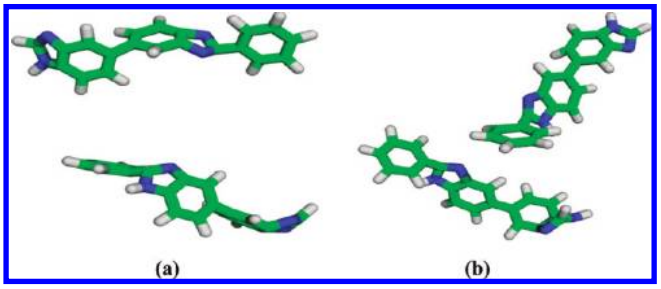

Figure 11. Snapshot of (a) parallel and (b) perpendicular orientation of BI molecules.

1:4 and 1:8 ratios to 1:14 ratio possibly helps in the proton conduction mechanisms of the PEMFC. This, however, is a matter of further investigation.

Dynamical Property: Ring Flipping and Diffusion. Further, to see the effect of stacking and H-bonding on the intramolecular rotation of BI molecules, the dihedral angle connecting two benzimidazole moieties, i.e., $C_4-C_5-C_{22}-C_{24}$ (atom numbers as in Figure 1a) is investigated, and a dihedral distribution plot is given in the Figure SI2 (Supporting Information). The flipping of the same dihedral of BI molecules were counted in each frame of the trajectory with respect to the angle between vectors connecting N_{33}, H_{34} and N_{37}, H_{38}. Flip was considered when the difference of the angle between the vectors was greater than 110° or less than −70° in consecutive frames taking into consideration the peak position in th edihedral distribution plot (Figure SI2, Supporting Information). The occurrence of flip count is shown in Figure 12. These occurrences for systems with different ratios of BI and PA were obtained from the last 10 ns trajectory of the production run and averaged over a number of BI molecules present in the system. The flipping is clearly observed to be very frequent in the case of the pure system, but the mixed systems do not have a large affinity for flipping. The smaller flipping tendency in the case of the mixed systems can again be attributed to the H-bonding with PA. Though H-bonding

dx.doi.org/10.1021/jp301117m | J. Phys. Chem. B 2012, 116, 7357−7366

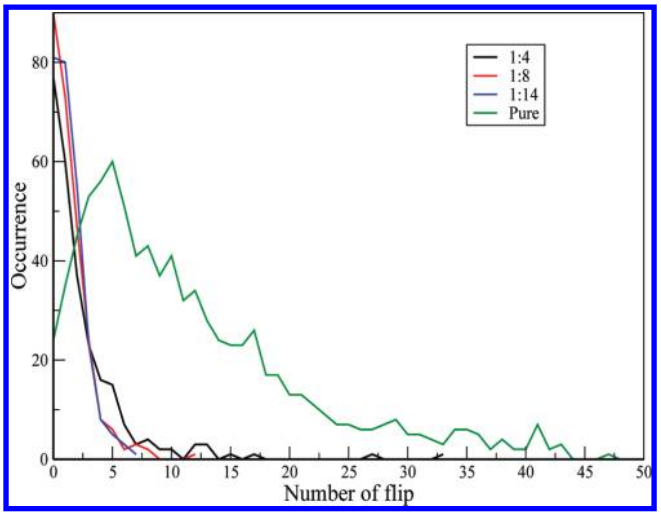

Figure 12. Occurrence of flipping per molecule over the 10 ns trajectory.

among the BI molecules exists in the pure BI system, such H-bonding is not as strong and not networked as with the PA in the mixed systems. Also, the absence of peaks at 0° or 180° in the stacking angle (Figure 10) can also be understood from flipping. The lesser tendency of the BI molecules for flipping in any of the mixed systems indicates the biasness toward a particular orientation of the BI molecules due to the presence of PA.

Proton conductivity in a PEM is also dependent upon the dynamical properties of its constituents. Hence, the self-diffusion of BI and PA in the BI−PA matrix has been calculated from the mean square displacement (MSD) for all mixed systems, which is depicted in Figure 13. The MSD curves for BI and PA clearly show that BI and PA molecules move much faster with the increase in the amount of PA. The diffusion constants were calculated for each mixed systems and reported in Table SI3 in the Supporting Information for quantitative understanding. We observe that the diffusion coefficient value of pure PA is one order of magnitude higher than pure BI. Experimentally, it was detected that proton conductivity increases with the increasing amount of PA.[21,30] It is also spotted from our simulation that the diffusion of PA increases (which will certainly increase the conductivity due to diffusion) with the increase in PA content in the mixed system. However, from Table SI3, Supporting Information, we observe that the diffusion coefficient value for PA in the 1:4 BI−PA system is ∼23 times less than the pure PA system and for BI, in the same mixed system, ∼4 times less than in pure system, but with an increase in PA content, i.e., for the 1:8 and 1:14 systems, the diffusion constant for both PA and BI got increased. To explain this initial drop of diffusion constant due to mixing, we have performed some additional simulations at lower PA ratios (BI−PA: 1:0.12, 1:0.25, 1:0.5, 1:1, and 1:2) and calculated the diffusion coefficient values for BI for each system at 500 K. The plot of diffusion coefficients as a function of PA ratio ranging from 0.12 to 14 is shown in Figure 14a. The diffusion coefficient of pure BI at 500 K is $1.03 \pm 0.38 \times 10^{-7}$ cm^2/s. With the addition of a small amount of PA, the diffusion coefficient value decreases, and it continues to decrease until 1:4 ratio, and beyond this ratio with the increase in PA ratio, the diffusion coefficient value increases. To explain this type of unusual behavior of the system, we have calculated the number of PA molecules forming bridging H-bonds with BI molecules. We have considered only those PA as bridging PA molecules whose two or three H's are forming H-bonds with BI molecules. For counting bridging PA molecules forming bridging H-bonds, we have used H-bond criterion, i.e., the distance between N atoms of BI and H atoms of PA should be less than or equal to 0.25 nm (in accordance with the RDF plots of Figure 6, $N_{33,35}$−HP), and additionally, the OS−HP−$N_{33,35}$ angle should be greater than 150°. Then, we have calculated the number of PA molecules forming two or three H-bonds with BI molecules. This calculation was performed from the last 10 ns trajectory of the production run and normalized by the total number of frames as the number of BI molecules are constant (64) in all the BI−PA mixed systems. We have plotted the number of bridging PA molecules as a function of PA ratio (with respect to BI) in Figure 14b. It is evident from the figure that, in between the 1:0.12 to 1:4 BI−PA ratios (i.e., small concentration of PA), the number of PA molecules having bridging H-bonds between PA and BI increases as the amount of PA increases, but with further increase in PA content, it decreases sharply. A higher number of bridging PA indicates the formation of a networked structure with the BI molecules, which make the system less mobile. Therefore, the diffusion coefficient value decreases, but with the increase of PA content, i.e., from the 1:4 to 1:14 ratio, the amount of bridging H-bonds with BI decreases. This may be due to presence of a higher number of PA molecules, which

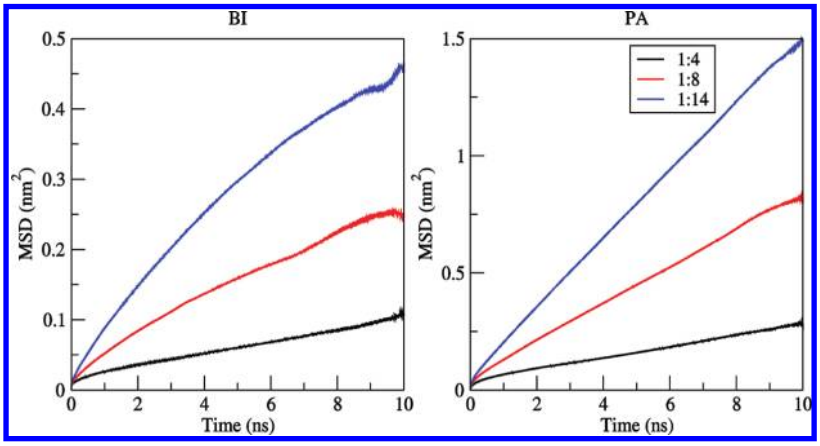

Figure 13. (a) MSD of BI in mixed systems. (b) MSD of PA in mixed systems.

dx.doi.org/10.1021/jp301117m | J. Phys. Chem. B 2012, 116, 7357−7366

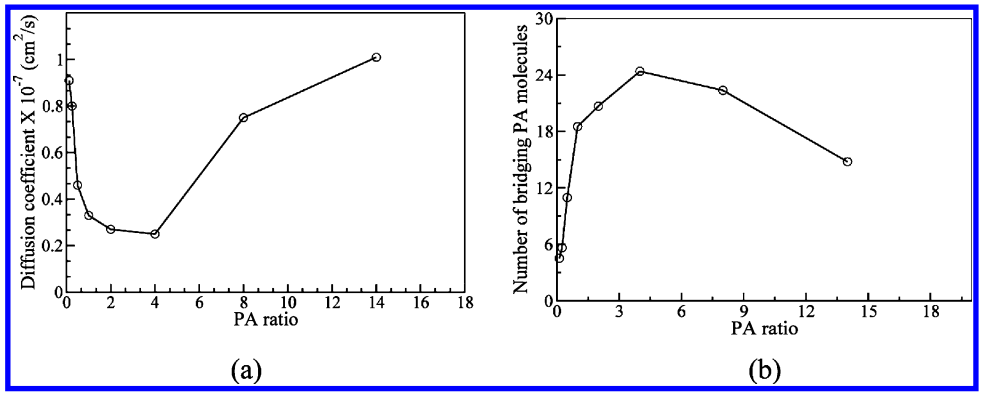

Figure 14. (a) Plot of diffusion coefficient values and (b) number of bridging PA molecules as a function of PA ratio.

favors the H-bonding of PA with themselves. Therefore, the possibility of formation of the bridging H-bond with BI decreases. As a consequence, mobility of PA and BI increases.

We have observed from the clustering of BI molecules (Figure 8) that, with the increase in the amount of PA molecules, clustering among the BI molecules decreases, and their tendency to remain as a single entity H-bonded with PA increases. This is possibly the reason for the increase in the diffusion coefficient values with an increase in the amount of PA beyond the 1:4 BI–PA ratio. Though the MSDs are shown only for 500 K (Figure 13), the diffusion constant values are reported for 400 and 450 K also (Table SI3, Supporting Information). The diffusion constant values were observed to increase with the increase in temperature.

CONCLUSIONS

The structural and dynamical properties of BI–PA mixtures at different doping levels of PA have been investigated using classical MD simulations. The mixture does not phase separate in any of the mixed systems; PA molecules were observed to form highly ordered H-bonded structures among themselves and also with the BI at all the BI to PA ratios. This ordering of PA around BI molecules increases with the increasing amount of PA. Cluster formation among the BI molecules was analyzed, and the cluster sizes of BI were observed to decrease with the increase in the PA doping level. This enables the H-bonding between PA and BI to be more feasible. The BI molecules were also observed to undergo stacking interactions and arrange in parallel and perpendicular orientations among themselves. However, there is a significant probability of the BI molecules to orient themselves at any angle among themselves. All this understanding will be useful to address the proton conduction in a PEMFC at its structural level. The present study gives us ample scope to be extended to PBI and hence better understanding of proton conduction at the structural level. The present study can be treated as a benchmark for such study. The force field used here and the structural understanding obtained equip us to deal with the mechanism of proton conduction in a much more sophisticated manner. There is further scope to understand the proton conduction mechanism at the structural level using ab initio molecular dynamics. This can also be useful to verify the proton conduction mechanism at various structural arrangements of PBI and PA. All of this understanding will help in the development of better and more efficient fuel cell membranes in the future.

ASSOCIATED CONTENT

Supporting Information

All bonded force field parameters for BI, charges of all the atoms of BI obtained from quantum chemical calculation, diffusion constant of BI and PA at different temperatures, fitting of the dihedral potential energy and dihedral distribution plots for $C_4–C_5–C_{22}–C_{23}$ and $C_{12}–C_{11}–C_7–N_{35}$ dihedrals, snapshot of a BI–PA mixed (1:4) system containing 512 BI and 2048 PA molecules, density and diffusion of pure bulk PA system (containing 2000 PA molecules) as a function of temperature. This material is available free of charge via the Internet at http://pubs.acs.org.

AUTHOR INFORMATION

Corresponding Author

*Phone: +91 20 2590 2735. Fax: +91 20 2510 2615. E-mail: s.roy@ncl.res.in.

Notes

The authors declare no competing financial interest.

ACKNOWLEDGMENTS

S.R. acknowledges the Center for Excellence in Scientific Computing, NCL, Pune for significant computational time. S.R. gratefully acknowledges the network project (project code NWP-22) for financial support for the project. A.V. acknowledges the Department of Science and Technology (SR/S1/PC/28/2009), India, and Department of Science and Technology, Nanomission (SR/NM/NS-42/2009), India, for financial assistance provided towards this work.

REFERENCES

(1) Crabtree, G. W.; Dresselhaus, M. S.; Buchanan, M. V. *Phys. Today* **2004**, *57*, 39–44.
(2) Venkatnathan, A.; Devanathan, R.; Dupuis, M. *J. Phys. Chem. B* **2007**, *111*, 7234–7244.
(3) Hogarth, W. H. J.; Diniz da Costa, J. C.; Lu, G. Q. *J. Power Sources* **2005**, *142*, 223–237.
(4) He, R.; Li, Q.; Bach, A.; Jensen, J. O.; Bjerrum, N. J. *J. Membr. Sci.* **2006**, *277*, 38–45.
(5) Ge, S.; Yi, B.; Ming, P. *J. Electrochem. Soc.* **2006**, *153*, A1443–A1450.
(6) Cheah, M. J.; Kevrekidis, I. G.; Benziger, J. *J. Phys. Chem. B* **2011**, *115*, 10239–10250.
(7) Suresh, G.; Scindia, Y. M.; Pandey, A. K.; Goswami, A. *J. Membr. Sci.* **2005**, *250*, 39–45.
(8) Neves, L. S. A.; Sebastião, P. J.; Coelhoso, I. M.; Crespo, J. G. *J. Phys. Chem. B* **2011**, *115*, 8713–8723.
(9) Hsu, W. Y.; Gierke, T. D. *J. Membr. Sci.* **1983**, *13*, 307–326.

(10) Devanathan, R.; Venkatnathan, A.; Dupuis, M. *J. Phys. Chem. B* **2007**, *111*, 13006−13013.
(11) Yan, L.; Zhu, S.; Ji, X.; Lu, W. *J. Phys. Chem. B* **2007**, *111*, 6357−6363.
(12) Moilanen, D. E.; Spry, D. B.; Fayer, M. D. *Langmuir* **2008**, *24*, 3690−3698.
(13) Roy, S.; Ataol, T. M.; Mu̇ller-Plathe, F. *J. Phys. Chem. B* **2008**, *112*, 7403−7409.
(14) Zhai, Y.; Zhang, H.; Zhang, Y.; Xing, D. *J. Power Sources* **2007**, *169*, 259−264.
(15) Yang, C.; Costamagna, P.; Srinivasan, S.; Benziger, J.; Bocarsly, A. B. *J. Power Sources* **2001**, *103*, 1−9.
(16) Kim, Y.-T.; Song, M.-K.; Kim, K.-H.; Park, S.-B.; Min, S.-K.; Rhee, H.-W. *Electrochim. Acta* **2004**, *50*, 645−648.
(17) Kwak, S.-H.; Yang, T.-H.; Kim, C.-S.; Yoon, K. H. *Electrochim. Acta* **2004**, *50*, 653−657.
(18) Kim, Y. M.; Choi, S. H.; Lee, H. C.; Hong, M. Z.; Kim, K.; Lee, H.-I. *Electrochim. Acta* **2004**, *49*, 4787−4796.
(19) Li, Q.; He, R.; Jensen, J. O.; Bjerrum, N. J. *Chem. Mater.* **2003**, *15*, 4896−4915.
(20) He, R.; Li, Q.; Jensen, J. O.; Bjerrum, N. J. *J. Polym. Sci., Part A: Polym. Chem.* **2007**, *45*, 2989−2997.
(21) Qingfeng, L.; Hjuler, H. A.; Bjerrum, N. J. *J. Appl. Electrochem.* **2001**, *31*, 773−779.
(22) Mamlouk, M.; Scott, K. *Int. J. Energy Res.* **2011**, *35*, 507−519.
(23) Wainright, J. S.; Wang, J. T.; Weng, D.; Savinell, R. F.; Litt, M. *J. Electrochem. Soc.* **1995**, *142*, L121−L123.
(24) Hu, J.; Zhang, H.; Zhai, Y.; Liu, G.; Yi, B. *Int. J. Hydrogen Energy* **2006**, *31*, 1855−1862.
(25) Chung, T.-S. *J. Macromol.Sci., Part C: Polym. Rev.* **1997**, *37*, 277−301.
(26) Li, Q.; He, R.; Berg, R. W.; Hjuler, H. A.; Bjerrum, N. J. *Solid State Ionics* **2004**, *168*, 177−185.
(27) He, R.; Che, Q.; Sun, B. *Fibers Polym.* **2008**, *9*, 679−684.
(28) Mecerreyes, D.; Grande, H.; Miguel, O.; Ochoteco, E.; Marcilla, R.; Cantero, I. *Chem. Mater.* **2004**, *16*, 604−607.
(29) Xiao, L.; Zhang, H.; Scanlon, E.; Ramanathan, L. S.; Choe, E.-W.; Rogers, D.; Apple, T.; Benicewicz, B. C. *Chem. Mater.* **2005**, *17*, 5328−5333.
(30) Kim, T.-H.; Lim, T.-W.; Lee, J.-C. *J. Power Sources* **2007**, *172*, 172−179.
(31) Li, Q.; He, R.; Jensen, J. O.; Bjerrum, N. J. *Fuel Cells* **2004**, *4*, 147−159.
(32) Stonehart, P. *Int. J. Hydrogen Energy* **1984**, *9*, 921−928.
(33) Asensio, J. A.; Sanchez, E. M.; Gomez-Romero, P. *Chem. Soc. Rev.* **2010**, *39*, 3210−3239.
(34) He, R.; Li, Q.; Xiao, G.; Bjerrum, N. J. *J. Membr. Sci.* **2003**, *226*, 169−184.
(35) Chin, D.-T.; Chang, H. *J. Appl. Electrochem.* **1989**, *19*, 95−99.
(36) Kerker, M.; Espenscheid, W. F. *J. Am. Chem. Soc.* **1958**, *80*, 776−779.
(37) Munson, R. A. *J. Phys. Chem.* **1964**, *68*, 3374−3377.
(38) Vilčiauskas, L.; Tuckerman, M. E.; Bester, G.; Paddison, S. J.; Kreuer, K.-D. *Nat. Chem.* **2012**, *4*, 461−466.
(39) Van Der Spoel, D.; Lindahl, E.; Hess, B.; Groenhof, G.; Mark, A. E.; Berendsen, H. J. C. *J. Comput. Chem.* **2005**, *26*, 1701−1718.
(40) Hess, B.; Kutzner, C.; van der Spoel, D.; Lindahl, E. *J. Chem. Theory Comput.* **2008**, *4*, 435−447.
(41) Jorgensen, W. L.; Tirado-Rives, J. *J. Am. Chem. Soc.* **1988**, *110*, 1657−1666.
(42) Jorgensen, W. L.; Maxwell, D. S.; Tirado-Rives, J. *J. Am. Chem. Soc.* **1996**, *118*, 11225−11236.
(43) Frisch, M. J.; Trucks, G. W.; Schlegel, H. B.; Scuseria, G. E.; Robb, M. A.; Cheeseman, J. R.; Scalmani, G.; Barone, V.; Mennucci, B.; Petersson, G. A.; Nakatsuji, H.; Caricato, M.; Li, X.; Hratchian, H. P.; Izmaylov, A. F.; Bloino, J.; Zheng, G.; Sonnenberg, J. L.; Hada, M.; Ehara, M.; Toyota, K.; Fukuda, R.; Hasegawa, J.; Ishida, M.; Nakajima, T.; Honda, Y.; Kitao, O.; Nakai, H.; Vreven, T.; Montgomery, J. A., Jr.; Peralta, J. E.; Ogliaro, F.; Bearpark, M.; Heyd, J. J.; Brothers, E.; Kudin, K. N.; Staroverov, V. N.; Kobayashi, R.; Normand, J.; Raghavachari, K.; Rendell, A.; Burant, J. C.; Iyengar, S. S.; Tomasi, J.; Cossi, M.; Rega, N.; Millam, J. M.; Klene, M.; Knox, J. E.; Cross, J. B.; Bakken, V.; Adamo, C.; Jaramillo, J.; Gomperts, R.; Stratmann, R. E.; Yazyev, O.; Austin, A. J.; Cammi, R.; Pomelli, C.; Ochterski, J. W.; Martin, R. L.; Morokuma, K.; Zakrzewski, V. G.; Voth, G. A.; Salvador, P.; Dannenberg, J. J.; Dapprich, S.; Daniels, A. D.; Farkas, O.; Foresman, J. B.; Ortiz, J. V.; Cioslowski, J.; Fox, D. J. *Gaussian 09*, revision A.1; Gaussian, Inc.: Wallingford, CT, 2009.
(44) Breneman, C. M.; Wiberg, K. B. *J. Comput. Chem.* **1990**, *11*, 361−373.
(45) Berendsen, H. J. C.; Postma, J. P. M.; van Gunsteren, W. F.; DiNola, A.; Haak, J. R. *J. Chem. Phys.* **1984**, *81*, 3684−3690.
(46) Kirkwood, J. G. *J. Chem. Phys.* **1934**, *2*, 351−361.
(47) Onsager, L. *J. Am. Chem. Soc.* **1936**, *58*, 1486−1493.
(48) Kumbharkar, S. C.; Karadkar, P. B.; Kharul, U. K. *J. Membr. Sci.* **2006**, *286*, 161−169.
(49) Ma, Y. L.; Wainright, J. S.; Litt, M. H.; Savinell, R. F. *J. Electrochem. Soc.* **2004**, *151*, A8−A16.